Journal of Solid State Chemistry 181 (2008) 1492–1505

Contents lists available at ScienceDirect

Journal of Solid State Chemistry

journal homepage: www.elsevier.com/locate/jssc

Anion substitution effects on the structure and magnetism of the chromium chalcogenide Cr_5Te_8—Part III: Structures and magnetism of the high-temperature modification $Cr_{(1+x)}Q_2$ and the low-temperature modification $Cr_{(5+x)}Q_8$ (Q = Te, Se; Te:Se = 5:3)

Joseph Wontcheu [a], Wolfgang Bensch [a,*], Sergiy Mankovsky [b], Svitlana Polesya [b], Hubert Ebert [b], Reinhard K. Kremer [c], Eva Brücher [c]

[a] Institute of Inorganic Chemistry, Christian-Albrechts-University Kiel, Olshausenstr. 40, D-24098 Kiel, Germany
[b] Department of Chemistry, LMU Munich, Butenandstr. 3-13, D-81377 Munich, Germany
[c] Max-Planck Institut für Festkörperforschung, Heisenbergstr. 1, D-70506 Stuttgart, Germany

ARTICLE INFO

Article history:
Received 20 June 2007
Received in revised form
27 February 2008
Accepted 5 March 2008
Available online 27 March 2008

Keywords:
Chromium chalcogenide
Anion substitution
Rietveld refinement
Magnetic properties
Spin-glass
SPR-KKR
Band-structure calculations

ABSTRACT

The title compounds were synthesized via the high-temperature (HT) route. The materials are characterized by Rietveld analysis, magnetic measurements, and electronic band-structure calculations. Two different structural modifications depending on the synthesis conditions are observed: a HT modification with trigonal basic cells (space group: $P\bar{3}m1$) for $Cr_{(1+x)}Q_2$ ($(1+x) = 1.25, 1.28, 1.34, 1.37, 1.41, 1.43$) and a low-temperature (LT) modification with trigonal super-cell (space group: $P\bar{3}m1$) for $Cr_{(5+x)}Q_8$ ($(5+x) = 5.00, 5.12, 5.36, 5.48, 5.64, 5.72$). The crystal structures are closely related to the NiAs-type structure with metal vacancies in every second metal layer. The substitution of Te by Se and the change of the Cr concentration induce significant alterations of the magnetic properties. With increasing Cr content the Weiss constant θ changes drastically from negative to strong positive values, i.e., with increasing Cr concentration a shift from predominant antiferromagnetic exchange to ferromagnetic exchange occurs. At LTs a complex magnetic behavior is observed. For some members a spin-glass (SG) behavior is found with the freezing temperature T_f following the Vogel–Fulcher law. At the highest Cr concentrations ferromagnetic characteristics dominate with spontaneous magnetizations below the Curie temperatures. The differences of the magnetic properties of the LT and HT phases can be explained on the basis of interatomic distances and angles. For a deeper understanding of the experimental results, they have been compared with the results of spin polarized relativistic Korringa–Kohn–Rostoker electronic band-structure calculations and both results are consistent. To explain the features of temperature-dependent magnetization of the compounds, Monte Carlo (MC) simulations based on the Heisenberg model have been performed with the exchange coupling parameters obtained within the *ab-initio* calculations of the electronic structure. The possible reasons for a modification of the exchange coupling parameters responsible for the temperature-dependent features are also analyzed.

1. Introduction

Chromium chalcogenides belong to the group of compounds with metal-deficient NiAs-type crystal structures and have significant theoretical importance as two-dimensional (2D) compounds with fastidious band structures and physical properties [1–5]. For the Cr–Te system, several phases were reported, i.e., $Cr_{1\pm x}Te$, $CrTe_2$, Cr_2Te_3, Cr_3Te_4, dimorphic Cr_5Te_8 and $CrTe_3$ which in general exhibit ferromagnetic behavior [6]. Regarding binary Cr sulfides and selenides, the phases CrS, Cr_2S_3, Cr_3S_4, Cr_5S_6, Cr_5S_8 [7–10], as well as $Cr_{1-x}Se$, Cr_3Se_4, Cr_2Se_3, Cr_5Se_8 [11–15] were studied which are antiferromagnetic showing electric conductivities of poor metals or semiconductors. The structures of these compounds can be viewed as layer-like structures with the Cr ions sandwiched between chalcogen layers. In all phases the Cr atoms are surrounded by six chalcogen atoms yielding a more or less distorted octahedral environment. The CrQ_6 (Q = S, Se, Te) octahedra located in neighbored layers share common faces

* Corresponding author. Fax: +49 4341 880 1520.
E-mail address: wbensch@ac.uni-kiel.de (W. Bensch).

0022-4596/$ - see front matter © 2008 Elsevier Inc. All rights reserved.
doi:10.1016/j.jssc.2008.03.021

yielding short Cr–Cr contacts. The interlayer direct exchange interaction is therefore stronger than exchange interactions within the layers which are of the superexchange type.

Studies of solid ternary solutions $Cr_{(5+x)}Te_{8-y}Se_y$ ($y = 1$, 2, $x = 0.08$, 0.28, 0.44) have shown that variations of the concentration of the components alter the magnetic properties ranging from antiferromagnetic, ferromagnetic, spin-glass (SG), cluster-glass (CG) or re-entrant spin-glass (RSG) behavior [16–18]. It has also been demonstrated that depending on the synthesis conditions, two structural modifications are obtained namely, trigonal super-cells (space group $P-3m1$) for $Cr_{(5+x)}Te_{8-y}Se_y$ (low-temperature (LT) modification) and trigonal basic cells with space group $P-3m1$ for $Cr_{(1+x)}Te_{2-y}Se_y$ (high-temperature (HT) modification) [17,18]. In $Cr_{(5+x)}Te_{8-y}Se_y$ the Cr atoms are located on four crystallographically unique sites leading to the formation of a five-layer super-structure of the CdI_2 type [16]. The $Cr_{(1+x)}Te_{2-y}Se_y$ structure contains only two Cr sites and can be regarded as a NiAs-type structure with metal atoms removed from every second metal atom layer [19]. $Cr_{(5+x)}Te_7Se$ and $Cr_{(5+x)}Te_6Se_2$ were investigated in our laboratory and we demonstrated that the substitution of Te by Se provokes remarkable changes of the crystal structures and magnetic properties [17,18]. Further substitution of 3 Te by Se should moreover alter the electronic situation and should continue changing the resulting physical properties dramatically. Therefore we present in this report the structural and magnetic properties of the new members $Cr_{(5+x)}Te_5Se_3$ ($x = 0.00$, 0.12, 0.36, 0.48, 0.64, 0.72, LT modification) and $Cr_{(1+x)}Te_{1.25}Se_{0.75}$ ($x = 0.25$, 0.28, 0.34, 0.37, 0.41, 0.43, HT modification). In addition results of accompanying theoretical investigations are presented that allow a rather detailed discussion of the achieved results.

2. Experimental details

2.1. Synthesis

The compounds $Cr_{(1+x)}Q_2$ ($x = 0.25$, 0.28, 0.34, 0.37, 0.41, 0.43 with Q = Te:Se in 5:3 ratio) with HT modifications crystallizing in trigonal basic cells have been prepared by direct solid state reactions. Mixtures of Cr (99.99%, Heraeus), Te (99.5%, Retorte), and Se (99.99%, Retorte) in the corresponding proportions were heated in evacuated sealed silica tubes to 950 °C at a rate of 100 °C/h and held at this temperature for 6 days, followed by subsequent cooling to 800 °C at a rate of 100 °C/h and held at this temperature for 2 days, and finally quenched to room-temperature in a water bath.

The LT modifications with trigonal super-cells $Cr_{(5+x)}Q_8$ ($x = 0.00$, 0.12, 0.36, 0.48, 0.64, 0.72) were prepared by annealing the $Cr_{(1+x)}Q_2$ samples. The $Cr_{(1+x)}Q_2$ compounds were crushed and loaded into silica tubes which were subsequently evacuated and sealed. The temperature was raised to 950 °C at a rate of 100 °C/h and held at this temperature for 2 days. The temperature was then decreased to 450 °C at a rate of 16 °C/h and held at this temperature for 6 days followed by quenching into a water bath.

In both cases, the products consist of polycrystalline black platelets with a metallic luster. The phase purity of the compounds was verified by X-ray diffraction and subsequent Rietveld refinements.

2.2. Composition analysis

The chemical compositions of the samples were determined first with EDX. The presence of all three elements corresponding to the average composition: $Cr_{1.25}Q_2/Cr_{5.00}Q_8$, $Cr_{1.28}Q_2/Cr_{5.12}Q_8$, $Cr_{1.34}Q_2/Cr_{5.36}Q_8$, $Cr_{1.37}Q_2/Cr_{5.48}Q_8$, $Cr_{1.41}Q_2/Cr_{5.64}Q_8$, $Cr_{1.43}Q_2/Cr_{5.72}Q_8$, was proved. Finally, the compositions were confirmed by means of inductively coupled plasma analysis (ICP) with an accuracy of about 2%.

2.3. X-ray powder diffraction and Rietveld refinement

X-ray powder diffraction patterns were recorded in transmission mode with a STOE Stadi-P diffractometer equipped with a linear position sensitive detector (PSD) and Ge monochromator using Cu$K\alpha$ radiation ($\lambda = 1.54056$ Å). The angular range of 2θ was 10–90° with 2θ step size of 1° and a counting time of 850 s for each step. The structure refinement was carried out with the Rietveld method [20–23] using the program Fullprof [24]. The results confirm that all the samples are homogeneous. The background of the experimental data was interpolated linearly between selected points. Examples of the final Rietveld refinement plots are shown in Fig. 1a for $Cr_{5.48}Q_8$ and $Cr_{1.37}Q_2$. Powder patterns of the HT phase (I) with that of the LT modification (II) are compared in Fig. 1b. The shape of the reflections was modeled with a pseudo-Voigt function. Preferred orientation was treated using March's function. The atomic coordinates were refined without constraints, whereas the atomic displacement parameters B_{iso} for Cr and all Te/Se atoms were tied during the refinement. The refinement of the HT phases was performed based on two crystallographically independent Cr sites (Cr(1) at 1*a* and Cr(2) at 1*b*, Table 2) and chalcogen atoms were statistically distributed over the 2*d* sites with the ratio of Te:Se fixed to 5:3. The isotropic displacement parameters for Cr(1) and Cr(2) were constrained to be the same in order to adjust the occupation factor of Cr(2). The occupancy of Cr(1) as well as that of Te/Se was not refined. For the LT modification, the starting values for the atomic positions were those of the trigonal Cr_5Te_8 structure in space group $P-3m1$ [25]. We carefully analyzed whether Te and Se atoms exhibit a preference for one of the four independent sites. Initially, refinements were performed only either with Te or Se to obtain the B_{iso} for these atoms giving hints for a site preference. Within the limits of the Rietveld method and the strong correlation between several parameters (B_{iso}, site occupation factors, absorption, texture) no significant differences of the B_{iso} could be detected. Therefore, refinements were done in the following way: Te and Se were statistically distributed over the four sites with the assumption that the Te:Se ratio is equal to 5:3 on each site. The results of the refinements are summarized in Tables 1a and b. Atomic coordinates and equivalent isotropic displacement parameters for representative compositions of the LT and HT modifications are presented in Table 2. Standard deviations of the refined parameters have been multiplied by the Bérar–Lelann factor [26].

2.4. Magnetic measurements

Magnetic measurements were conducted with a physical properties measurement system (PPMS) or a MPMS SQUID magnetometer. The dc susceptibilities were measured in the temperature range of $4.2\,K \leqslant T \leqslant 300\,K$ with a field of 0.1 T. The zero-field cooled (ZFC) and field-cooled (FC) magnetizations M_{ZFC} and M_{FC} were taken at 26, 60, 100 and 1000 Oe as follows. The system was cooled in zero field to 4.2 K, a corresponding field was set immediately after $T = 4.2$ K was reached, and M_{ZFC} data taken on warming from 4.2 to 300 K; finally M_{FC} data recorded on cooling from 300 to 4.2 K with a field. The ac susceptibilities were measured at 10, 100 and 1000 Hz with a field of 5 Oe. Field-dependent magnetizations were recorded for $Cr_{1.28}Q_2/Cr_{5.12}Q_8$ and $Cr_{1.43}Q_2/Cr_{5.72}Q_8$ at 15.0 K with a field up to 9 T.

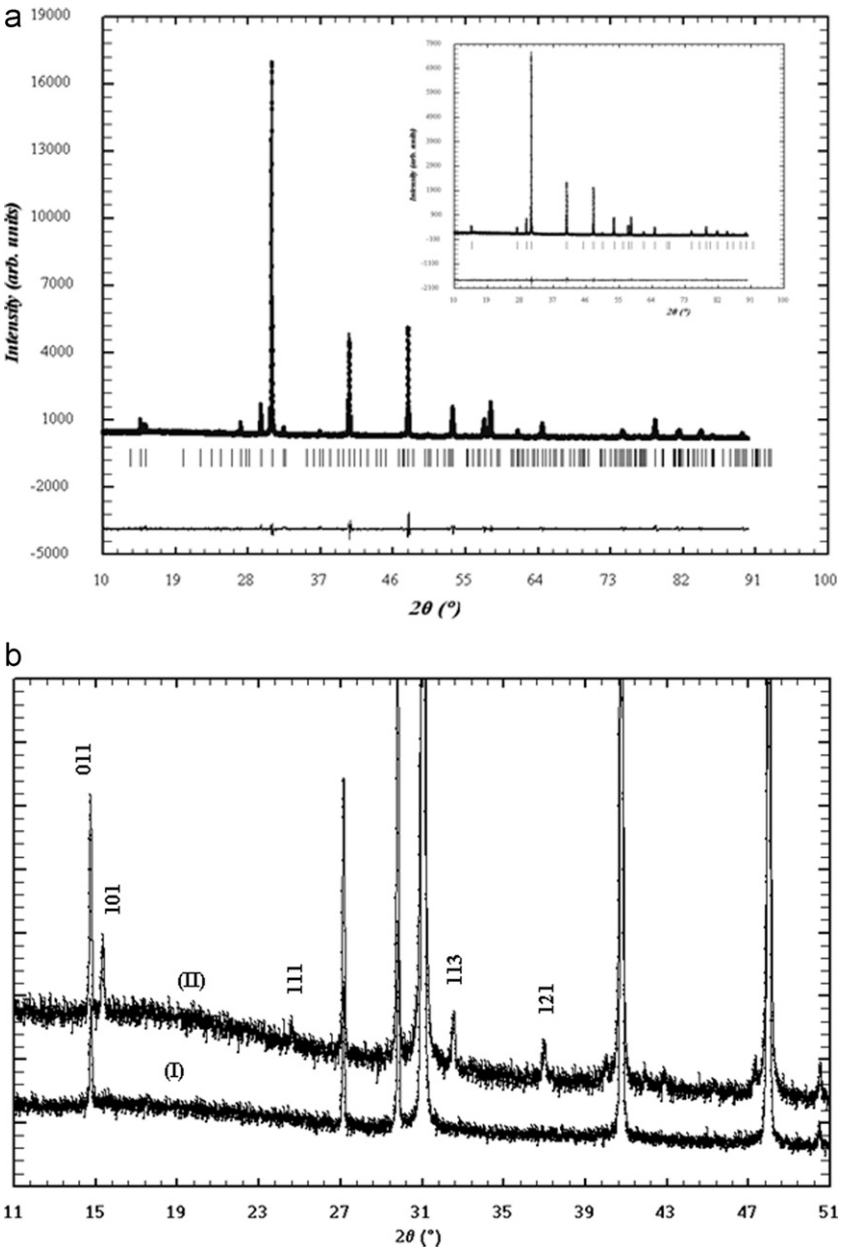

Fig. 1. (a) Rietveld refinement plot of $Cr_{5.48}Q_8$ (inset: $Cr_{1.37}Q_2$) X-ray data with peak markers and difference plot at the bottom. (b) Powder patterns of the high temperature phase (I) and the low temperature modification (II).

2.5. Theoretical investigations

To support the interpretation of our experimental results accompanying calculations have been done on the electronic and magnetic properties of the investigated compounds. The electronic structure calculations for $Cr_{(1+x)}Q_2$ have been performed using the spin polarized relativistic Korringa–Kohn–Rostoker (SPR-KKR) band-structure method in the atomic sphere approximation (ASA) mode [27–30]. Exchange and correlation were treated within the framework of the local spin-density approximation (LSDA) of spin-density functional theory, using the parametrisation of Vosko et al. [31]. To describe the chemical disorder within the chalcogen sub-lattice, as well as the random distribution of vacancies within the Cr sub-lattice, the coherent potential approximation (CPA) alloy theory was used [32,33]. Because of the rather large unit cell of the $Cr_{(5+x)}Q_8$ system we focused the calculations on the $Cr_{(1+x)}Q_2$ system.

To study the magnetic properties at finite temperature Monte Carlo (MC) simulations have been performed which is based on the classical Heisenberg model. The effective exchange coupling parameters J_{ij} have been calculated using the expression derived by Lichtenstein et al. [34] on the basis of magnetic force theorem. The MC simulations have been done by cooling gradually the alloy system from a HT using a lattice spanned by $6 \times 6 \times 6$ cells with periodic boundary conditions. The exchange interaction of Cr magnetic moments with all neighbors within a sphere with radius R_{max} equal to three times the lattice parameter a were taken into account.

3. Results and discussion

3.1. Crystal structures

The crystal structures of $Cr_{(1+x)}Q_2$ ($x = 0.25$, 0.28, 0.34, 0.37, 0.41, 0.43) are closely related to the NiAs-type and consists of

Table 1a
Crystal data and structure refinement results for $Cr_{(1+x)}Q_2$ Q = (Te, Se; Te:Se = 5:3)

Formula	$Cr_{1+x}Q_2$					
(1+x)	1.25	1.28	1.34	1.37	1.41	1.43
Crystal system	Trigonal					
Space group	$P-3m1$					
a (Å)	3.787(1)	3.795(1)	3.798(1)	3.800(1)	3.804(1)	3.805(2)
c (Å)	5.981(1)	6.005(2)	6.011(1)	6.029(1)	6.049(1)	6.057(1)
V (Å^3)	74.265(2)	74.904(1)	75.075(2)	75.414(2)	75.824(1)	75.924(2)
Z	1					
2θ range (deg)	10–90					
N_{obs}	38	36	38	38	40	40
N_{ref}	13	13	13	13	13	13
R_{wp}	7.59	6.16	5.43	7.28	9.12	9.14
R_e	7.18	5.61	4.88	6.86	6.79	4.73
χ^2	1.81	2.11	1.95	1.77	2.45	3.76
DW	1.329	1.322	1.229	1.345	0.978	0.414
R_{Bragg}	3.98	2.66	3.90	3.55	5.02	4.91
R_F	5.63	4.27	6.49	5.28	4.69	6.77

Table 1b
Crystal data and structure refinement results for $Cr_{(5+x)}Q_8$ Q = (Te, Se; Te:Se = 5:3)

Formula	$Cr_{5+x}Q_8$					
(1+x)	5.00	5.12	5.36	5.48	5.64	5.72
Crystal system	Trigonal					
Space group	$P-3m1$					
a (Å)	7.569(1)	7.577(1)	7.580(1)	7.590(1)	7.596(1)	7.624(1)
c (Å)	11.970(1)	12.006(1)	12.019(1)	12.051(1)	12.079(1)	12.119(1)
V (Å^3)	593.94(2)	596.94(4)	598.00 (3)	601.26(4)	603.49(3)	610.01(5)
Z	2					
2θ range (deg)	10–90					
N_{obs}	213	217	217	217	217	219
N_{ref}	23	23	23	23	23	23
R_{wp}	5.51	7.22	5.60	7.11	6.42	5.66
R_e	4.91	6.73	4.93	5.22	4.44	3.38
χ^2	1.26	1.25	1.39	1.92	2.02	2.96
R_{Bragg}	4.96	4.59	3.01	3.63	3.96	3.65
R_F	9.74	9.11	8.63	9.85	7.74	11.20

Table 2
Atomic coordinates, site occupation factors (sof) and isotropic displacement parameter B_{iso} for representative $Cr_{(1+x)}Q_2$ and $Cr_{(5+x)}Q_8$ compounds

Atom	Site	x	y	z	B_{iso} (Å^2)	sof
$Cr_{1.37}Q_2$						
Cr(1)	1a	0	0	0	5.24	1
Cr(2)	1b	0	0	1/2	5.24	0.372
Te(1)	2d	1/3	2/3	0.2505(2)	4.63	0.625
Se(1)	2d	1/3	2/3	0.2505(2)	4.63	0.375
$Cr_{5.48}Q_8$						
Cr(1)	1b	0	0	0	3.69(10)	0.918(4)
Cr(2)	6i	0.4853(5)	0.5147(5)	0.2532(15)	3.69(10)	1
Cr(3)	2c	0	0	0.243(2)	3.69(10)	1
Cr(4)	3e	0	1/2	0	3.69(10)	0.681(6)
Te(1)	2d	1/3	2/3	0.3933(10)	4.14(3)	0.625
Te(2)	2d	2/3	1/3	0.1339(13)	4.14(3)	0.625
Te(3)	6i	0.1706(5)	0.8294(5)	0.1224(7)	4.14(3)	0.625
Te(4)	6i	0.8356(5)	0.1644(5)	0.3726(9)	4.14(3)	0.625
Se(1)	2d	1/3	2/3	0.3933(10)	4.14(3)	0.375
Se(2)	2d	2/3	1/3	0.1339(13)	4.14(3)	0.375
Se(3)	6i	0.1706(5)	0.8294(5)	0.1224(7)	4.14(3)	0.375
Se(4)	6i	0.8356(5)	0.1644(5)	0.3726(9)	4.14(3)	0.375

chalcogen layers stacked upon each other perpendicular to the c-axis. They define octahedral sites alternatively occupied by Cr(1) and Cr(2) leading to the real stacking sequence

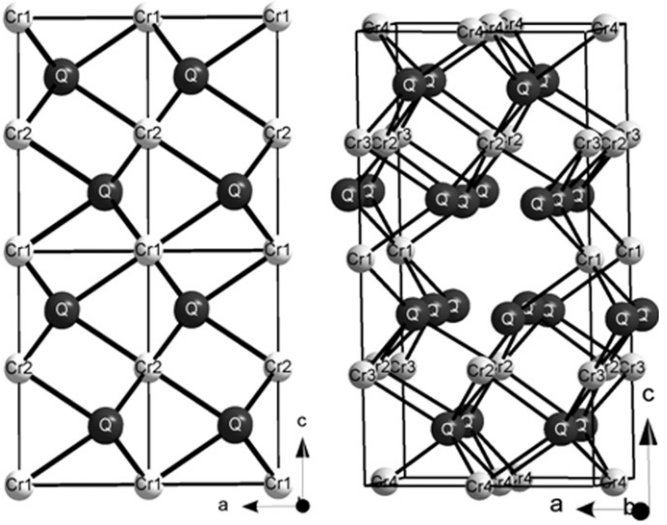

Fig. 2. Crystal structure of trigonal $Cr_{(1+x)}Q_2$ with basic cell (a) and trigonal $Cr_{(5+x)}Q_8$ with super-cell (b).

⋯–Q–Cr(1)–Q–Cr(2)–Q–Cr(1)–⋯ (Fig. 2, left), with the Cr(2) site being only partially occupied. Within the full layers, Cr(1)Q_6 octahedra share common edges leading to intralayer Cr–Cr distances ranging from 3.79 to 3.81 Å (Table 3a). Along the c-axis, the CrQ_6 octahedra share common faces and the resulting interlayer Cr–Cr distances are with 2.99 and 3.03 Å much shorter than the intralayer Cr–Cr separations. The Cr(1)Q_6 and Cr(2)Q_6 octahedra are relatively regular with Cr–Q distances ranging from 2.654 to 2.668 Å and 2.643 to 2.665 Å, respectively, depending on the Cr content (Table 3a).

The crystal structures of $Cr_{(5+x)}Q_8$ (x = 0.00, 0.12, 0.36, 0.48, 0.64, 0.72) can be viewed as a derivative of the hexagonal NiAs-type structure with metal vacancies being located in every second metal atom layer perpendicular to the crystallographic c-axis (Fig. 2, right). The four crystallographically unique Cr atoms are in a distorted octahedral environment of 6 Q anions. The CrQ_6 octahedra in the fully occupied layers share common edges and long Cr–Cr separations (ranging from 3.470 to 4.120 Å for Cr(2)–Cr(2) and from 3.790 to 3.820 Å for Cr(2)–Cr(3) (Table 3a)) in the ab plane are observed. The Cr(1) and Cr(4) centered octahedra in the partially occupied layers are joined to the Cr(3) or Cr(2) octahedra via common faces. This leads to short Cr–Cr separations (spreading from 3.050 to 3.110 Å for Cr(2)–Cr(4) and from 3.060 to 3.120 Å for Cr(1)–Cr(3)) along the crystallographic c-axis (see Table 3a).

In many chromium chalcogenide compounds similar short metal-to-metal distances were observed, and examples are $CrTi_2Se_4$ (3.067 Å), $TiCr_2Se_4$ (3.101 Å) [35], $TlCr_5Se_8$ (3.059 Å) [36], $TlCr_5S_8$ (2.959 Å) [37], and Cr_4TiSe_8 (3.0058 Å) [38]. Such short Cr–Cr distances indicate weak bonding interactions between the metal centers. The Cr–Q bond lengths range from 2.550 to 2.820 Å (see Table 3a) with average interatomic Cr–Q bonds $\langle$Cr(1)–$Q\rangle$ = 2.660–2.685 Å, $\langle$Cr(2)–$Q\rangle$ = 2.550–2.820 Å, $\langle$Cr(3)–$Q\rangle$ = 2.650–2.700 Å and $\langle$Cr(4)–$Q\rangle$ = 2.620–2.750 Å (see Table 3a) being typical for Cr–Te/Se bonds [6–15]. An elongation of the average Cr–Q bonds is observed with increasing Cr content. The average Cr–Q distances scatter over a relatively large range indicating pronounced distortions of the CrQ_6 octahedra in the $Cr_{(5+x)}Q_8$ phases. Such distortions may probably deteriorate the coupling of magnetic moments and influence the magnetic properties of these compounds as discussed below.

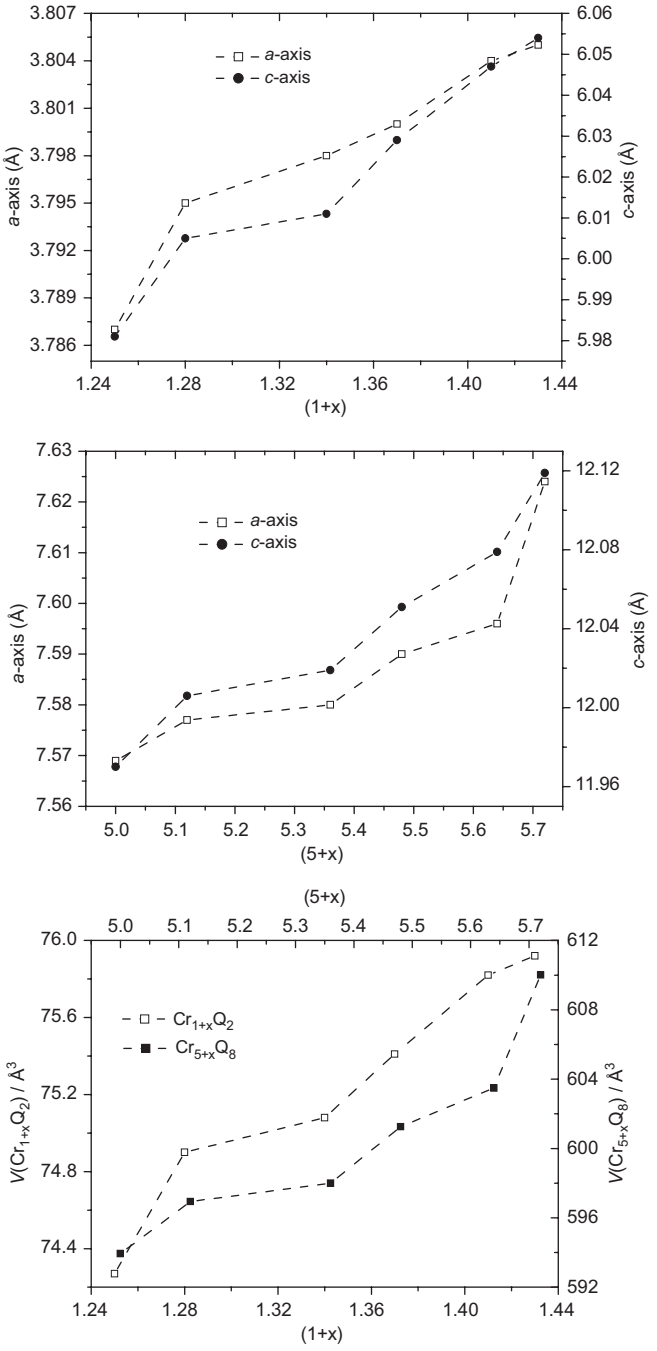

Fig. 3. Variation of the lattice parameters (a, c, V) with chromium concentration x in $Cr_{(1+x)}Q_2$ and $Cr_{(5+x)}Q_8$.

The variations of the lattice parameters a, c and V with Cr concentration x in $Cr_{(1+x)}Q_2$ and $Cr_{(5+x)}Q_8$ are presented in Fig. 3. With increasing Cr concentration the lattice parameters a and c as well as the volume V increase in both cases. The effect of the c-axis elongation is about two times larger than that of the a-axis, implying a significant expansion along this axis and finally a net increase of V with increasing Cr content occurs. Analyzing the alterations of the unit cell parameters more in detail two different regions can be distinguished. For chromium-rich compounds starting from $Cr_{1.34}Q_2/Cr_{5.36}Q_8$ up to $Cr_{1.43}Q_2/Cr_{5.72}Q_8$, the a- and c-axis and the unit cell volume V change in a fairly linear manner with the chromium content. In fact the electronic situation requires on the one hand mixtures of Cr(III) ($rCr^{3+} = 0.615$ Å) and Cr(IV) ($rCr^{4+} = 0.41$ Å) for compounds with lower Cr concentrations and on the other hand Cr(III) and Cr(II) ($rCr^{2+} = 0.73$ Å) for those with higher Cr contents [39]. The difference between the ionic radii of Cr(IV) and Cr(II) may explain the non-linearity in the investigated concentration range. A comparison of the lattice parameters of $Cr_{1.37}Q_2$ (Te:Se = 5:3, this work) with those of $Cr_{1.36}Q_2$ with a lower Se content (Te:Se = 6:2) [18] shows a net decrease with increasing Se content. For instance the a, c and V parameters are 3.843, 6.046 Å and 77.32 Å^3 for $Cr_{1.36}Q_2$ (Te:Se = 6:2) and 3.800, 6.029 Å, and 75.41 Å^3 for $Cr_{1.37}Q_2$ (Te:Se = 5:3). As expected the higher Se concentration yields a further contraction of the unit cell parameters. In the $Cr_{(5+x)}Te_{8-y}Se_y$ phases, the Cr atoms experience locally different direct and indirect magnetic exchange interactions due to the randomly distributed Te/Se atoms over the four crystallographically distinct sites and due to the disorder of the Cr atom distribution in the metal-deficient layers. The generated magnetic frustration may introduce CG, SG or SG-like behavior in the series of materials as discussed below.

3.2. Magnetic properties

The inverse magnetic susceptibilities vs. temperature between 4.2 and 300 K for $Cr_{(1+x)}Q_2$ and $Cr_{(5+x)}Q_8$ are displayed in Fig. 4. The numerical results obtained from fit with a Curie–Weiss law to the

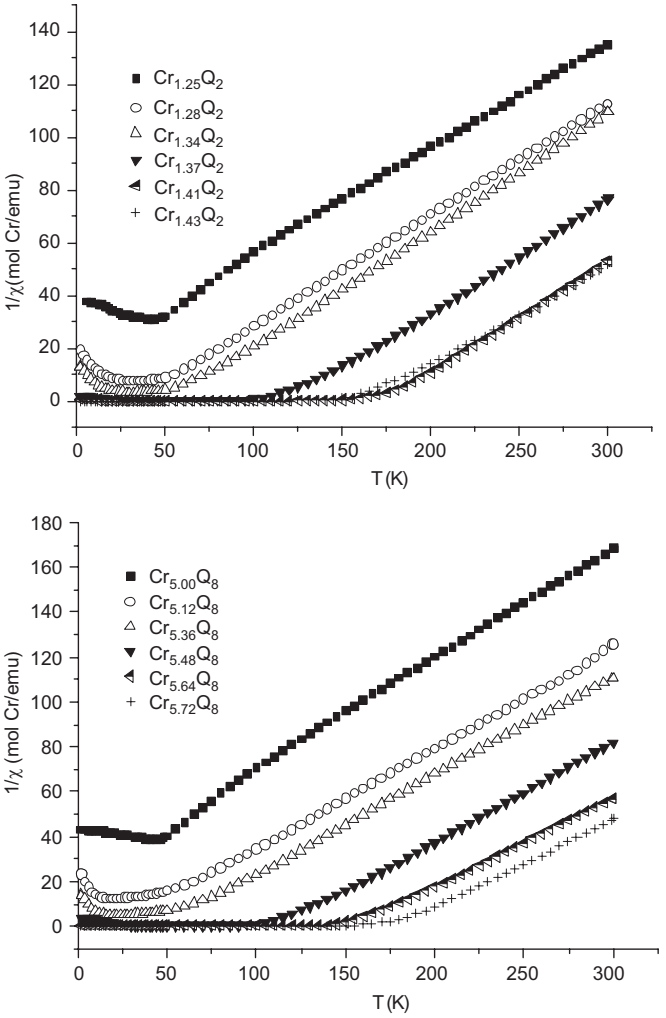

Fig. 4. Temperature dependencies of the inverse magnetic susceptibility measured in a field of 0.1 T of $Cr_{(1+x)}Q_2$ (upper panel) and $Cr_{(5+x)}Q_8$ (lower panel).

linear part of the reciprocal susceptibility are summarized in Table 4. In the fitting range (Table 4) all compounds follow the Curie–Weiss law with effective magnetic moments per Cr atom ranging from 4.06 to 4.53 μ_B/Cr. These values are larger than the expected spin-only value of 3.87 μ_B for Cr(III) in a high spin d^3 ($s = 3/2$) electronic configuration. However, several Cr chalcogenides have been found to exhibit magnetic moments larger than the spin-only value. Examples are $TlCr_5Se_8$ with 4.01 μ_B, $KCr_5Te_{7.8}$, with 4.46 μ_B, $TlCrTe_2$ with 4.47 μ_B, and $TlCr_5S_{8-y}Se_y$ with values between 3.92 and 4.25 μ_B [40]. Shimada et al. [41] attributed such enlarged magnetic moments to an electron transfer from Q to Cr via $d-p$ hybridization. In an ionic description the chromium poor samples may be formulated as containing mixtures of Cr^{4+} (d^2) and Cr^{3+} (d^3) cations. For instance $Cr_{1.28}Q_2/Cr_{5.12}Q_8$ may be written as $(Cr^{3+})_{1.12}(Cr^{4+})_{0.16}Q_2/(Cr^{3+})_{4.48}(Cr^{4+})_{0.64}Q_8$ and the expected magnetic moment should be lower than 3.87 μ_B. On increasing the chromium content the electronic balance requires the coexistence of Cr^{3+} and Cr^{2+} (d^4). As an example, $Cr_{1.41}Q_2/Cr_{5.64}Q_8$ may be formulated as $(Cr^{3+})_{1.18}(Cr^{2+})_{0.23}Q_2/(Cr^{3+})_{4.72}(Cr^{2+})_{0.92}Q_8$. Assuming Cr(II) to be in a high spin state the resulting magnetic moment will be larger than 3.87 μ_B. The validity of this simple ionic approach is certainly limited and a partial charge transfer from Q to Cr may better account for the experimentally determined enhanced magnetic moments.

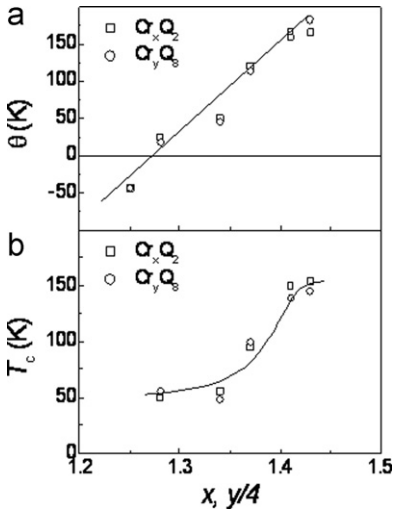

Fig. 5. (a) Weiss constant θ as extrapolated from the high temperature reciprocal magnetic susceptibility shown in Fig. 4 and (b) Curie temperature T_c derived from the magnetization traces displayed in Figs. 6, 10 and 11 of Cr_xQ_2 and Cr_yQ_8. The solid lines serve as guide to the eyes.

With increasing Cr concentration the Weiss constant θ drastically increases from −43 to 175 K ($Cr_{(1+x)}Te_{1.25}Se_{0.75}$ series) and from −47 to 179 K ($Cr_{(5+x)}Te_5Se_3$ series) (Fig. 5). In a first approximation, the Weiss constant θ measures the sum of the nearest neighbor exchange interactions, $\theta = S(S+1)/3k_B\Sigma_i z_i J_i$, where z_i is the number of nearest neighbors interacting with exchange J_i. The sign change of θ with increasing Cr content therefore indicates a shift from predominant antiferromagnetic exchange to ferromagnetic exchange interaction. Analyzing in detail the data of Tables 3a and b two different exchange paths are useful to explain the magnetic behavior. On one hand, the Cr–Cr distance between metal atoms located in adjacent layers increases from 2.99 to 3.03 Å in the $Cr_{(1+x)}Q_2$ series on going from $x = 0.25$ to 0.43 and from 3.05 to 3.12 Å in the $Cr_{(5+x)}Q_8$ series for $x = 0.00$ and 0.72, respectively (Table 3a). Such short Cr–Cr contacts support direct antiferromagnetic exchange interactions [42–44]. An increase of the Cr–Cr distance weakens this interaction. On the other hand, the Cr–Cr interatomic distances between metal atoms located within fully or partially occupied metal layers amount to 3.78–3.81 Å for $Cr_{(1+x)}Q_2$ ($x = 0.25$ to $x = 0.43$) and to 3.78–4.12 Å for $Cr_{(5+x)}Te_5Se_3$, respectively (cf. Table 3a). Such distances are too large for direct exchange. Indirect 90° superexchange via a Cr^{3+}–Q^{2-}–Cr^{3+} contact involving a partly-filled t_{2g} orbital of one cation, an empty e_g orbital of the second cation, and a doubly occupied p orbital of the anion, is preferred. Additionally, Cr–Q–Cr angles near 90° yield stronger ferromagnetic exchange interactions (Table 3b). Both mechanisms are simultaneously present and their balance depends on the interatomic metal–metal distances and Cr–Q–Cr angles. Comparing the compounds with approximately the same Cr content but different Te:Se ratios it is

Table 3a
Selected interatomic distances (Å) for $Cr_{(1+x)}Q_2$ and $Cr_{(5+x)}Q_8$

	$Cr_{1.25}Q_2$	$Cr_{1.28}Q_2$	$Cr_{1.34}Q_2$	$Cr_{1.37}Q_2$	$Cr_{1.41}Q_2$	$Cr_{1.43}Q_2$
Cr(1)–Cr(1)	3.7867(1)	3.7950(1)	3.7976(1)	3.8004(1)	3.8050(1)	3.8043(1)
Cr(2)–Cr(2)	3.7867(1)	3.7950(1)	3.7976(1)	3.8004(1)	3.8050(1)	3.8043(1)
Cr(1)–Cr(2)	2.9903(1)	3.0027(1)	3.0055(1)	3.0147(1)	3.0237(1)	3.0288(1)
Cr(1)–Q(1)	2.6544(11)	2.6642(10)	2.6612(17)	2.6637(11)	2.6680(10)	2.6630(9)
Cr(2)–Q(1)	2.6428(11)	2.6480(10)	2.6551(11)	2.6603(10)	2.6650(11)	2.6720(10)
	$Cr_{5.00}Q_8$	$Cr_{5.12}Q_8$	$Cr_{5.36}Q_8$	$Cr_{5.48}Q_8$	$Cr_{5.64}Q_8$	$Cr_{5.72}Q_8$
Cr(2)–Cr(2)	4.048(6)	4.050(7)	4.049(6)	4.066(7)	4.113(8)	4.114(8)
Cr(3)–Cr(2)	3.790(3)	3.794(3)	3.795(3)	3.801(3)	3.805(4)	3.820(4)
Cr(4)–Cr(4)	3.785(1)	3.789(1)	3.790(1)	3.795(1)	3.797(1)	3.812(1)
Cr(1)–Cr(3)	3.06(2)	3.06(2)	3.079(16)	3.10(2)	3.10(6)	3.11(2)
Cr(2)–Cr(4)	3.050(17)	3.078(16)	3.076(12)	3.082(17)	3.06(2)	3.109(17)
Cr(1)–Q(4) 6 ×	2.661(8)	2.762(8)	2.668(7)	2.660(7)	2.654(7)	2.684(8)
Cr(2)–Q(1) 1 ×	2.570(14)	2.557(15)	2.594(11)	2.619(13)	2.619(16)	2.624(14)
Cr(2)–Q(2) 1 ×	2.767(14)	2.791(14)	2.782(10)	2.774(12)	2.788(14)	2.818(13)
Cr(2)–Q(3) 2 ×	2.625(13)	2.649(12)	2.640(10)	2.630(12)	2.607(14)	2.638(13)
Cr(2)–Q(4) 2 ×	2.669(12)	2.658(11)	2.667(9)	2.684(12)	2.722(14)	2.694(12)
Average	2.654	2.660	2.665	2.670	2.678	2.684
Cr(3)–Q(3) 3 ×	2.651(14)	2.659(14)	2.659(11)	2.653(13)	2.676(14)	2.693(13)
Cr(3)–Q(4) 3 ×	2.657(15)	2.656(14)	2.671(12)	2.680(14)	2.670(16)	2.663(14)
Average	2.654	2.658	2.665	2.667	2.673	2.678
Cr(4)–Q(2) 2 ×	2.687(10)	2.681(10)	2.690(8)	2.713(8)	2.725(9)	2.729(9)
Cr(4)–Q(3) 4 ×	2.620(7)	2.622(7)	2.622(6)	2.633(6)	2.623(7)	2.629(6)
Average	2.642	2.642	2.645	2.660	2.657	2.663

Table 3b
Selected angles (deg) for $Cr_{(1+x)}Q_2$ and $Cr_{(5+x)}Q_8$

	$Cr_{1.25}Q_2$	$Cr_{1.28}Q_2$	$Cr_{1.34}Q_2$	$Cr_{1.37}Q_2$	$Cr_{1.41}Q_2$	$Cr_{1.43}Q_2$
⟨Cr(1)–Q–Cr(1)⟩	90.00(4)	90.00(4)	90.00(4)	90.00(4)	90.00(4)	90.00(4)
	91.01(5)	90.83(4)	91.04(4)	90.95(7)	91.06(4)	91.15(6)
⟨Cr(2)–Q–Cr(2)⟩	90.00(4)	90.00(4)	90.00(4)	90.00(4)	90.00(4)	90.00(4)
	91.51(5)	91.55(5)	91.31(4)	90.87(4)	91.10(7)	90.76(6)
	$Cr_{5.00}Q_8$	$Cr_{5.12}Q_8$	$Cr_{5.36}Q_8$	$Cr_{5.48}Q_8$	$Cr_{5.64}Q_8$	$Cr_{5.72}Q_8$
⟨Cr(2)–Q–Cr(2)⟩	87.7(4)	87.7(4)	87.4(3)	87.5(3)	87.3(4)	87.0(4)
	90.7(2)	92.4(4)	87.8(3)	91.6(4)	87.0(4)	87.5(5)
	92.6(4)	92.7(4)	93.4(3)	92.4(3)	93.1(5)	92.5(4)
⟨Cr(2)–Q–Cr(3)⟩	87.1(4)	87.0(4)	87.9(4)	87.8(5)	89.8(5)	86.3(4)
	90.7(4)	91.1(4)	90.6(3)	90.5(3)	89.1(6)	87.6(5)
	91.8(4)	91.2(4)	91.5(3)	91.4(5)	92.1(5)	91.5(4)
⟨Cr(4)–Q–Cr(4)⟩	89.4(2)	87.7(4)	89.3(2)	88.7(2)	88.4(3)	87.0(4)
	89.5(3)	92.4(4)	90.7(2)	91.9(4)	92.7(2)	93.0(4)

apparent that the antiferromagnetic exchange interactions grow with increasing Se content. For instance, the Weiss constant which was found to be 115 K for $Cr_{1.26}Te_{1.75}Se_{0.25}$ [17] drops to 53 K for $Cr_{1.27}Te_{1.5}Se_{0.5}$ [18], and finally reaches −43 K for $Cr_{1.25}Te_{1.25}Se_{0.75}$ or 32 K for $Cr_{1.28}Te_{1.25}Se_{0.75}$ (this work). These series demonstrate the complex interplay between Cr content and the interatomic distances and the trends observed in the magnetic properties described in the following. The magnitude of the magnetization, the Curie temperature T_c and the freezing temperature T_f are similarly related to the change of Cr content and the concomitant changes of the Cr–Cr distances and the Cr–*Q*–Cr angles.

The dependence of the HT susceptibility as reflected by the effective magnetic moments and the Weiss constant on the Cr content is also reflected in the LT behavior of the ZFC and FC magnetizations M_{ZFC} and M_{FC} of $Cr_{(1+x)}Q_2$ (HT) and $Cr_{(5+x)}Q_8$ (LT). Complex magnetic behavior is observed at LTs with some differences between the LT and the HT phase. In general, antiferromagnetic correlations prevail at lower Cr contents while towards the higher Cr contents, ferromagnetic behavior becomes dominant. In between, phases with the composition $Cr_{1.28}Q_2$ and $Cr_{5.12}Q_8$ have a Weiss constant θ not far from 0, i.e., nearly a compensation of ferro- and antiferromagnetic exchange occurs. For $Cr_{1.28}Q_2$ and $Cr_{5.12}Q_8$ SG behavior is observed. The ZFC susceptibility of $Cr_{1.28}Q_2$ shows a cusp while for $Cr_{5.12}Q_8$ the maximum in the ZFC susceptibility is rounded (Fig. 6). Similar to the dc magnetization, the maximum in the real part of the ac susceptibility of $Cr_{5.12}Q_8$ is markedly broadened and the temperature of the maximum shows a significantly increased frequency shift (Fig. 7). If we define the cusp temperature as the SG freezing temperature, T_f, its frequency shift follows nicely a Vogel–Fulcher law with a significantly larger frequency dependence of $1/T_f$ for $Cr_{5.12}Q_8$ as compared to that of $Cr_{1.28}Q_2$ (Fig. 8).

While the magnetizations of $Cr_{1.25}Q_2$ and Cr_5Q_8 decrease above the maximum indicative of antiferromagnetic correlations, the FC magnetization M_{FC} of $Cr_{1.28}Q_2$ and $Cr_{5.12}Q_8$ exhibit a moderate increase. Such a plateau-like behavior in the FC traces below T_f is seen in classic metallic SGs, such as CuMn and AuFe [45], as well as in insulating SGs, such as $Fe_{0.5}Mn_{0.5}TiO_3$ [46]. The shape of the magnetization curve and the reduced frequency dependence of T_f suggest that $Cr_{1.28}Q_2$ is closer to a ferromagnet, and SG-like behavior and ferromagnetism compete. The positive value for the Weiss constant (Table 4 and Fig. 5) is a further indication that ferromagnetic exchange prevails in this phase. The field dependence of the magnetization (Fig. 9) shows a linear increase of the magnetization at small fields. However, full saturation of the magnetization is not observed even at 9 T. This finding is in line with the proposed SG or SG-like behavior of the two compounds.

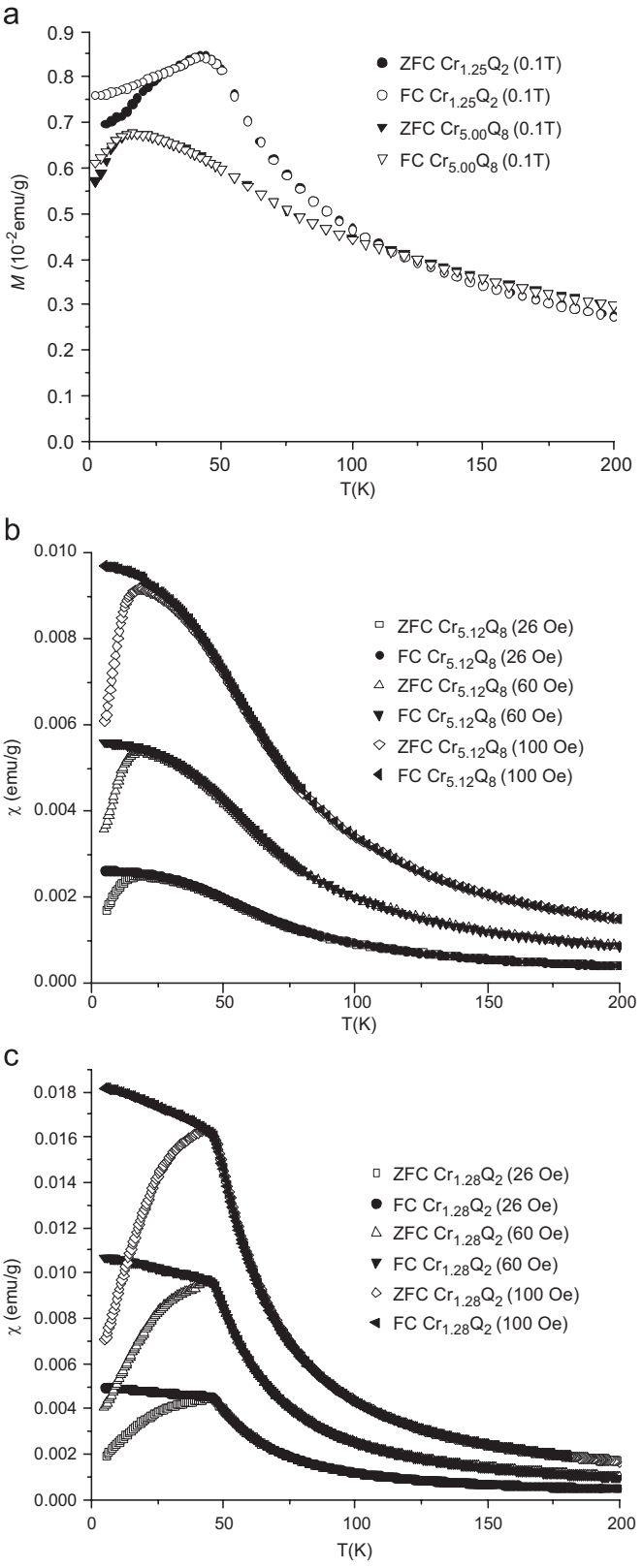

Fig. 6. Field cooled (FC) and zero-field cooled (ZFC) magnetization of samples given in the inset measured at fields as indicated.

As already indicated by the strongly growing and positive Weiss constants (Fig. 5a), the phases Cr_xQ_2 and Cr_yQ_8 with $x > 1.28$

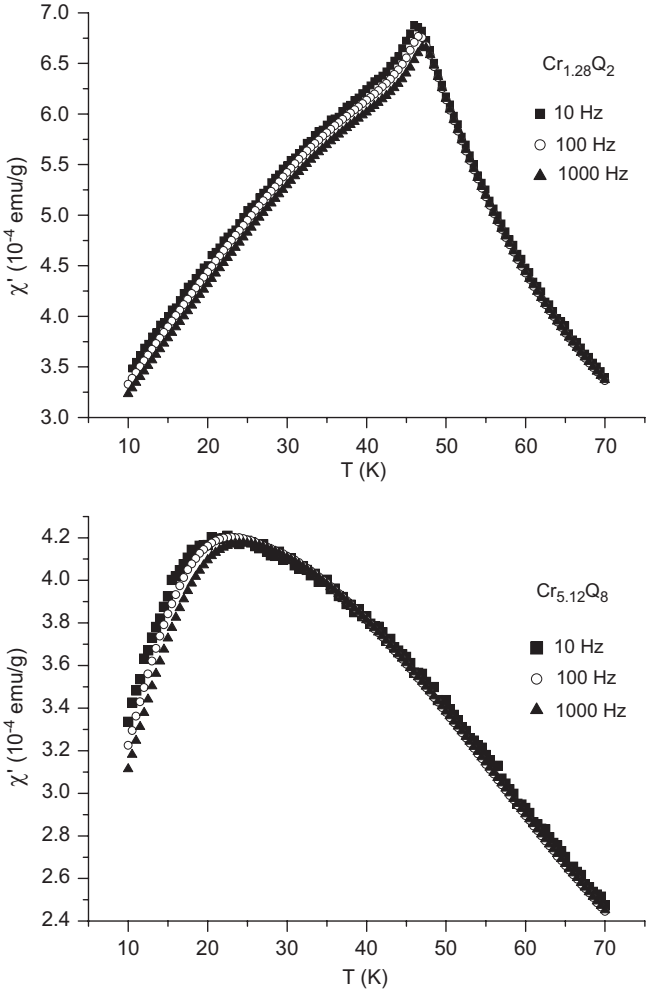

Fig. 7. Frequency dependence of the real part of the ac susceptibilities of $Cr_{1.28}Q_2$ and $Cr_{5.12}Q_8$ measured at frequencies as indicated in the inset.

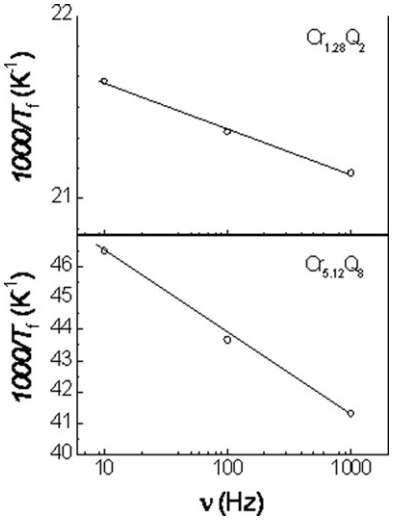

Fig. 8. Frequency dependence of the inverse freezing temperature $1/T_f$ as given by the cusp and the maximum temperatures of the real part of the ac susceptibilities displayed in Fig. 7.

and $y > 5.12$ exhibit a clear increase of ferromagnetic characteristics. The FC magnetizations show spontaneous magnetization below Curie temperatures T_c's taken as the maximum of the first derivative of the FC magnetizations (Figs. 10 and 11) with respect

Table 4
Magnetic characteristics for $Cr_{(1+x)}Q_2$ and $Cr_{(5+x)}Q_8$

	$Cr_{1.25}Q_2$	$Cr_{1.28}Q_2$	$Cr_{1.34}Q_2$	$Cr_{1.37}Q_2$	$Cr_{1.41}Q_2$	$Cr_{1.43}Q_2$
μ_{eff} (μ_B/Cr)	4.47	4.35	4.24	4.30	4.36	4.53
θ (K)	−43	32	56	123	168	175
H (T)	0.1	0.1	0.1	0.1	0.1	0.1
T_{min}/T_{max} (K)	100/300	100/300	100/300	170/300	200/300	230/300
T_c	–	≈50	60	125	175	175
	$Cr_{5.00}Q_8$	$Cr_{5.12}Q_8$	$Cr_{5.36}Q_8$	$Cr_{5.48}Q_8$	$Cr_{5.64}Q_8$	$Cr_{5.72}Q_8$
μ_{eff} (μ_B/Cr)	4.06	4.24	4.25	4.23	4.48	4.50
θ (K)	−47	24	48	117	156	174
H (T)	0.1	0.1	0.1	0.1	0.1	0.1
T_{min}/T_{max} (K)	100/300	100/300	100/300	170/300	200/300	200/300
T_c	–	≈45	48	120	160	180

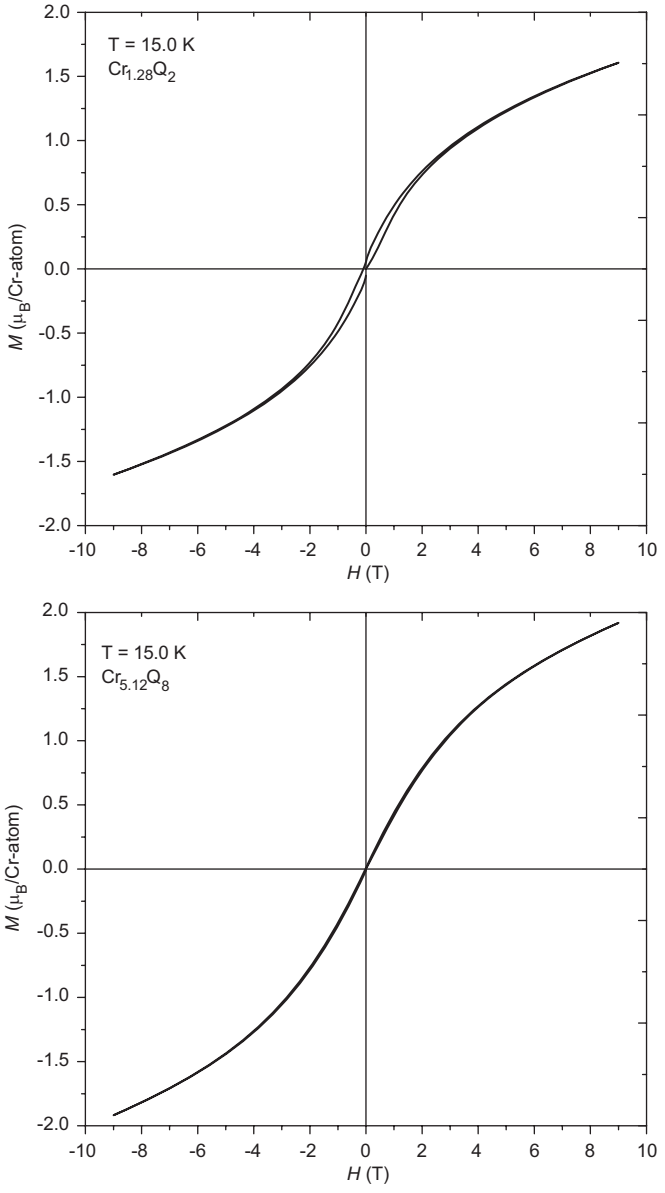

Fig. 9. Magnetic field dependence of the magnetizations of $Cr_{1.28}Q_2$ and $Cr_{5.12}Q_8$ measured at 15 K.

to field. With increasing x and y, T_c shows an S-shape dependence on x and y with a leveling off at ~150 K (Fig. 5b) for $x \geqslant 1.41$ and $y \geqslant 5.64$ and at ~50 K for $x \leqslant 1.34$ and $y \leqslant 5.36$. The splitting of the

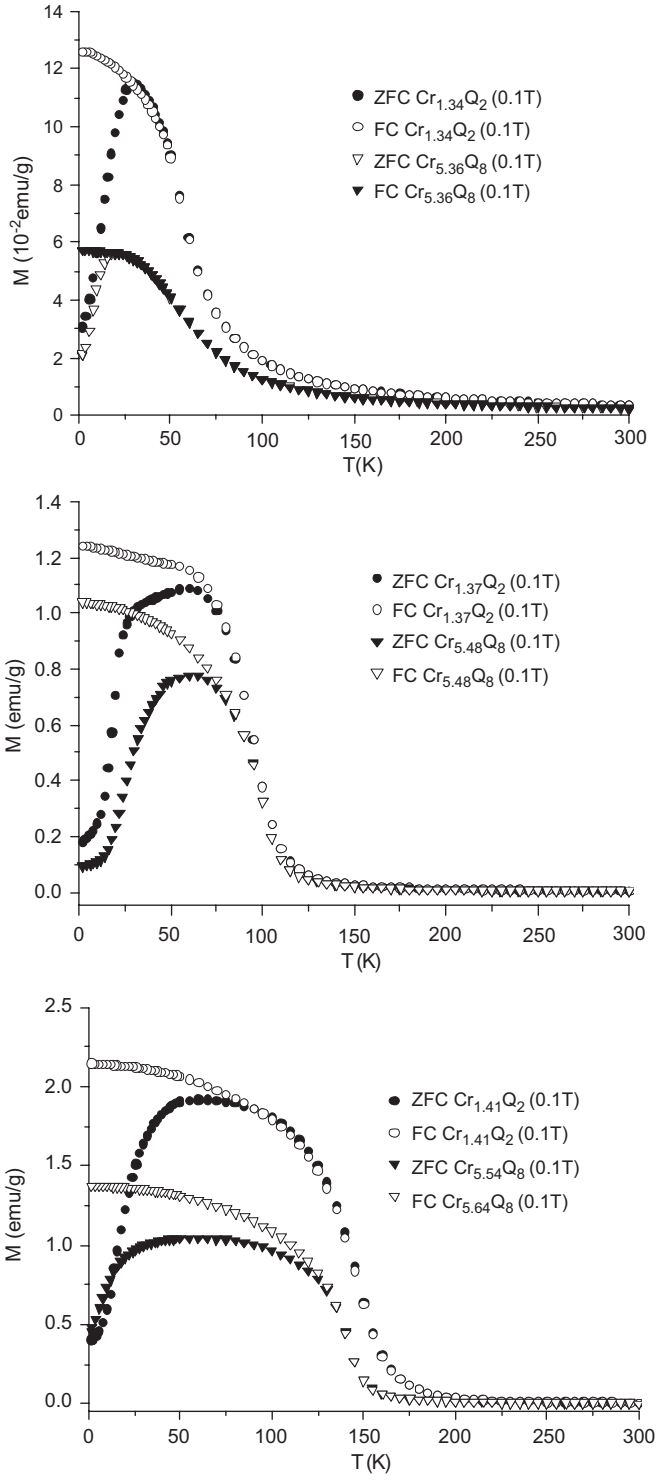

Fig. 10. FC and ZFC magnetic susceptibilities of $Cr_{1.34}Q_2$ and $Cr_{5.36}Q_8$, $Cr_{1.37}Q_2$ and $Cr_{5.48}Q_8$, and $Cr_{1.41}Q_2$ and $Cr_{5.64}Q_8$, from top to bottom, respectively, measured in a magnetic field of 0.1 T.

ZFC and the FC susceptibilities due to ferromagnetic domain formation when cooling in zero-field becomes more and more pronounced towards highest x and y indicative that the ferromagnetic phase becomes very homogeneous. For $x = 1.43$ and $y = 5.72$, the magnetization versus field shows typical saturation behavior of a ferromagnet with spontaneous ordering (Fig. 12).

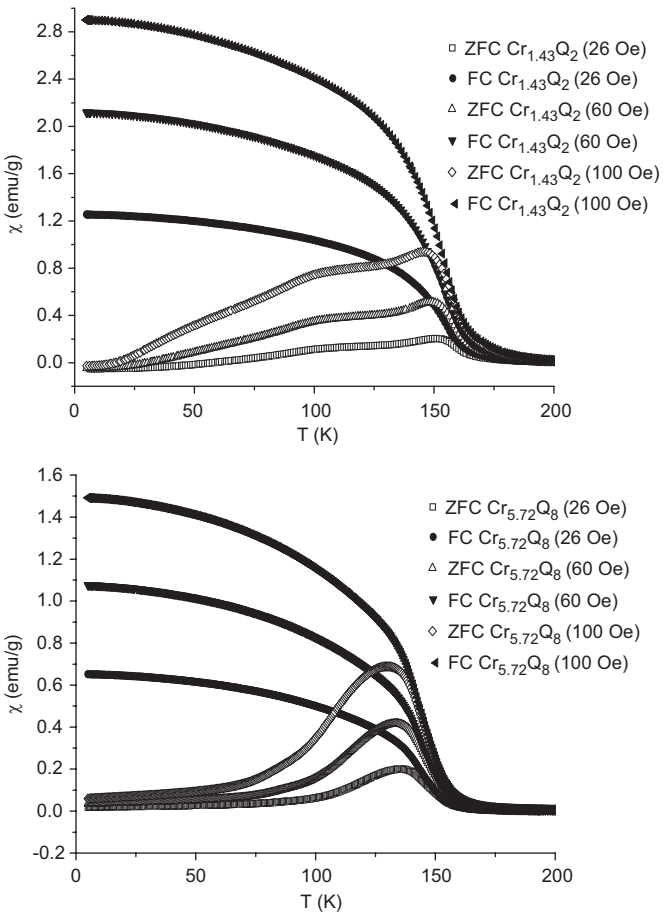

Fig. 11. Temperature dependencies of the FC and ZFC magnetic susceptibilities of $Cr_{1.43}Q_2$ and $Cr_{5.72}Q_8$ measured in magnetic fields as indicated.

In the complete magnetization loop a hysteresis is seen with 0.06 T ($Cr_{1.43}Q_2$), respectively, 0.03 T ($Cr_{5.72}Q_8$) as the coercitive fields, and 2.32 emu/g ($Cr_{1.43}Q_2$) and 1.20 emu/g ($Cr_{5.72}Q_8$) for the remanence. Such low values suggest the presence of soft ferromagnetic domains.

3.3. Band-structure calculations

The class of materials considered here shows an extremely rich variety concerning their structural and magnetic properties. As an example, our recent experimental results demonstrated an unexpected behavior for the magnetic transformation temperature as a function of Cr concentration. The possible reasons for these peculiarities were discussed above making a semi-empirical analysis of the exchange interactions, based on the so-called Goodenough–Kanamori–Anderson rules. To complement these qualitative considerations we present in the following results of *ab-initio* electronic structure calculations.

For these materials, this type of calculations is quite challenging for various reasons. First one has to mention that the Cr content in the compounds under consideration is non-stoichiometric, and one therefore has to clarify the site occupation within the Cr sub-lattice. This problem has been studied in detail and discussed in our previous works. It was found that for the most favorable occupation the Cr(1) sites are completely occupied while the Cr(2) sites are only occupied according to the average concentration. This means that the Cr sites create in the system two sub-lattices that are fully and partially occupied, respectively.

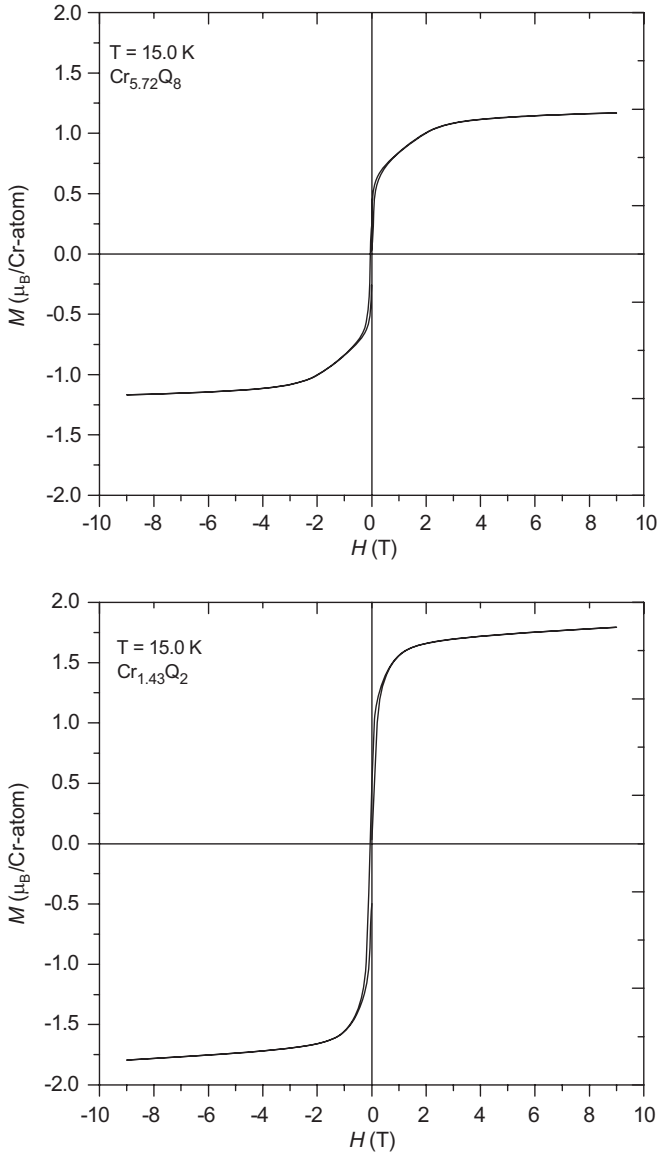

Fig. 12. Magnetic field dependence of the magnetizations of $Cr_{1.43}Q_2$ and $Cr_{5.72}Q_8$ measured at 15 K.

Accordingly, the Cr-subsystem can be considered as a system of alternating complete and incomplete Cr monolayers.

The lattice parameters and atomic coordinates within the unit cell can be determined theoretically on the basis of total energy calculations. However, this procedure requires large computational effort. Therefore only the optimization of the lattice parameter a has been performed while all other structural parameters (e.g. c/a ratio, atomic positions within the unit cell) have been taken from the experiment.

The total energy calculations, performed for optimized structural parameters, show that a magnetic configuration with antiparallel alignment of Cr(1) and Cr(2) spin magnetic moments is energetically more favorable than the ferromagnetic one. Table 5 represents the values of the spin magnetic moment for each component of the compounds. Obviously, the absolute values of the spin magnetic moments increase with the Cr concentration both for Cr(1) as well as Cr(2) atoms. However, the increase of the Cr(2) magnetic moment is much more pronounced than that of Cr(1). The induced Te and Se spin magnetic moments are negative and their absolute values decrease upon increase of Cr concentration. We already discussed above that this concentration

Table 5
Element resolved spin magnetic moments in $Cr_{(1+x)}Q_2$ as a function of Cr content

x	Cr(1)	Cr(2)	Te	Se
1.25	2.6325	−1.0982	−0.1236	−0.1776
1.34	2.6900	−1.2843	−0.1050	−0.1524
1.41	2.7883	−1.5346	−0.0952	−0.1405

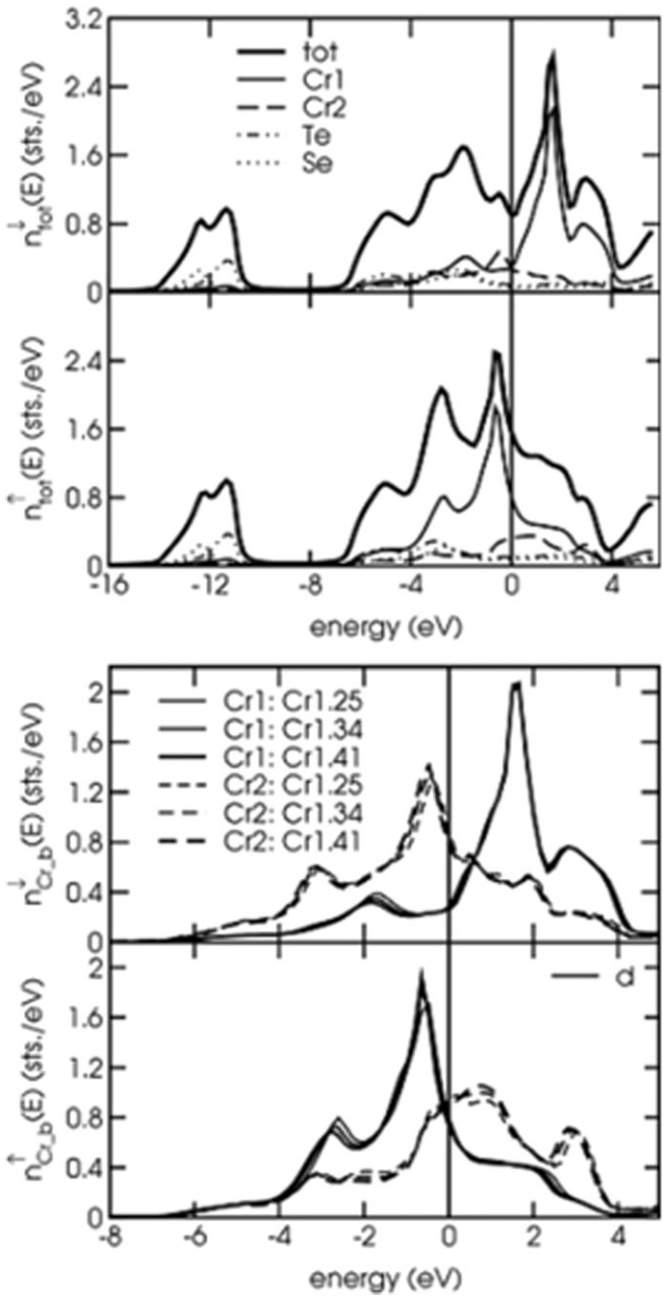

Fig. 13. Element resolved DOS for $Cr_{1.41}Q_2$ (Te:Se = 5:3) (top) and the DOS of d-states of Cr(1) and Cr(2) atoms at different Cr content ($1+x = 1.25$, 1.34, 1.41) (bottom).

dependence of the spin magnetic moments is related to the change in the hybridization of Te and Se p-states with the d-states of the two adjacent Cr layers. This can be followed by inspecting the corresponding density of states (DOS) curves.

Fig. 13 (top) shows only the total and element resolved DOS for $Cr_{1.41}Q_2$ (Te:Se = 5:3), as the other alloys possess very similar DOS

curves. The DOS curves of *d*-states of Cr(1) and Cr(2) atoms are compared with one another for different Cr content in Fig. 13 (bottom). As can be seen, an increase of Cr content results in a shift of the electronic states to higher binding energy. The exchange splitting of Cr(1) *d*-states is more pronounced than that of the Cr(2) *d*-states. This reflects the different spin magnetic moments as can be seen in Table 5. Fig. 13 (top) shows clearly that the electronic band structure is dominated in the valence band regime by the *d*-bands of the Cr atoms that hybridize with the chalcogen *p*-states. The semi-core band at higher binding energy, on the other hand, originates primarily from chalcogen *s*-states.

The present spin-polarized band-structure calculations based on spin-density functional theory allow only investigating the ground state of a system. The temperature-dependent magnetic properties in turn can be investigated using MC simulations based on the Heisenberg model of magnetism. While the *ab-initio* calculations are restricted to rather small unit cells as well as assume here only parallel or antiparallel alignments of the Cr magnetic moments, MC simulations can be used to deal with more complicated magnetic structures including a possibly non-collinear magnetic ground state of a system.

The exchange coupling parameters $J^{Cr1-Cr1}$, $J^{Cr1-Cr2}$ and $J^{Cr2-Cr2}$ required for these simulations were obtained within the KKR Green's function calculations for compounds with three different Cr concentrations. The corresponding results are presented in Fig. 14. In general, the behavior of these coupling parameters as a function of the Cr–Cr distance is very similar. In particular their magnitudes do not differ in an appreciable way except of the couplings with the first and second neighboring atoms. Comparing the present results with the previous ones obtained for samples with Te:Se = 6:2, one notices that the change of the Te:Se ratio does not influence the values of the exchange coupling parameters very much. This means that the temperature-dependent magnetic properties of these systems should be quite similar. Indeed this could be demonstrated by our MC simulations. According to these, the total magnetic moment increases slowly upon cooling, reaching a maximum in the vicinity of the critical temperature. The following temperature decrease is accompanied by a decrease of the average spin magnetic moment. Thus, according to the present MC simulations, the system exhibits upon cooling a transition to a state with antiferromagnetic order within the fully occupied Cr(1) sub-lattice (see Fig. 15). The incomplete Cr(2) sub-lattice with the random distribution of Cr atoms does not exhibit any magnetic order approaching to $T = 0$ K. This means that one could indeed expect a SG-like behavior of the alloys under consideration, related to a corresponding SG-like behavior of magnetic moments of incomplete Cr(2) sub-lattice. An increase of the Cr concentration leads to an increase of the probability for the Cr(2) atoms to be arranged close to each other and to create in this way magnetically ordered clusters, as one can see in Fig. 15. Accordingly, a CG-like behavior can indeed be expected for $Cr_{(1+x)}Q_2$ systems at LTs.

The critical temperatures obtained with the MC simulation are compared with the experimental results in Fig. 16. In contrast to our previous results for $Cr_{(1+x)}Q_2$ with the ratio Te:Se = 6:2, showing a very good agreement between theoretical and experimental results, the theoretical results reproduce the experimental data only in a qualitative way. To understand the reason for these unexpected features related to the change in the Te:Se ratio, one has obviously to analyze the properties of the exchange coupling parameters. As already mentioned above, the dependence of the exchange coupling parameters on the Cr content is rather weak and should be responsible for a pronounced modification of the corresponding critical temperatures.

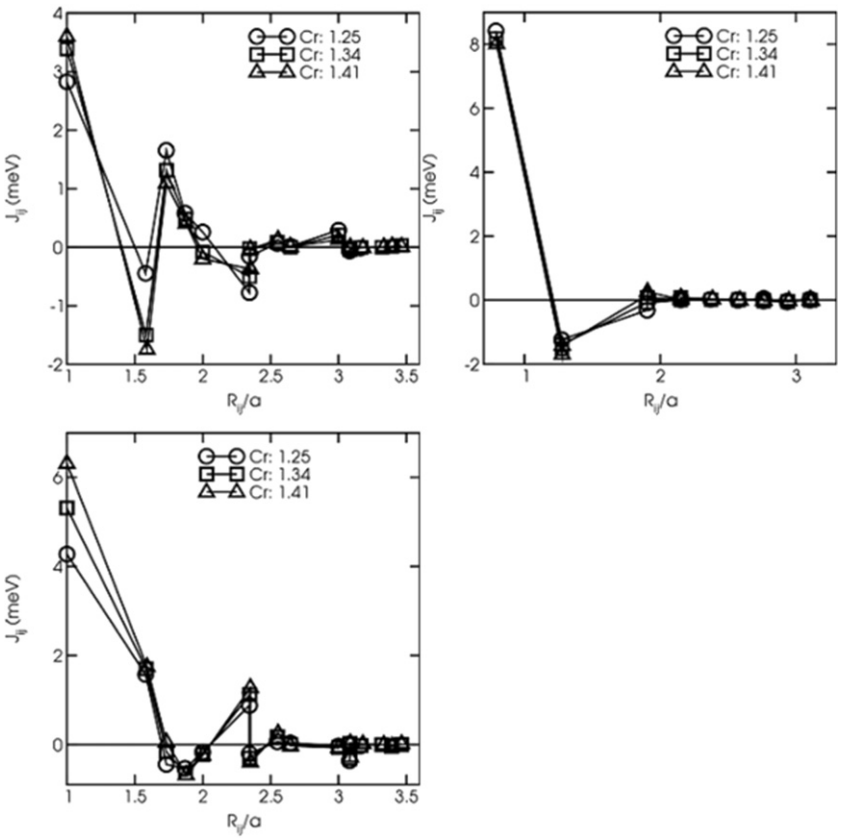

Fig. 14. Calculated exchange coupling parameters $J^{Cr1-Cr1}$, $J^{Cr1-Cr2}$ and $J^{Cr2-Cr2}$, for the compounds $Cr_{(1+x)}Q_2$ with $(1+x) = 1.25$, 1.34, 1.41. The inter-atomic distances are represented in units of lattice parameters *a*.

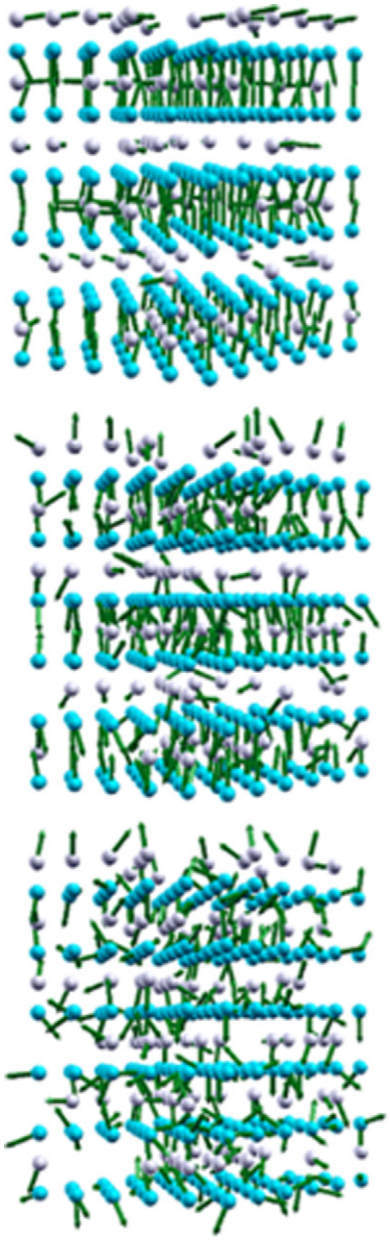

Fig. 15. Spin magnetic structures at the temperatures 1 K (a), 50 K (b) and 150 K (c), obtained within the MC simulations.

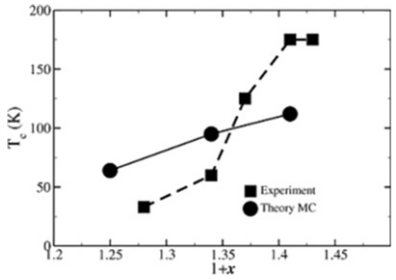

Fig. 16. Critical temperatures obtained within the MC simulation (circles) as a function of Cr content, compared with the experimental results (squares).

Considering the $J^{Cr1-Cr1}$, $J^{Cr1-Cr2}$ and $J^{Cr2-Cr2}$ exchange couplings between the first and second neighbors as a function of the band filling (see Fig. 17), one can see that they strongly vary in the vicinity to the Fermi level corresponding to the respective Cr concentrations ($1+x = 1.25, 1.34, 1.41$). However, due to the high DOS of Cr *d*-electrons at these energies, a shift of the Fermi level caused by a variation of the Cr concentration is small enough to result in the large changes of the exchange coupling parameters.

The role of the (Te,Se) sub-lattice was already discussed within the semi-empirical approach and it was pointed out that the *s*- and *p*-electrons of Te and Se are essentially involved into the exchange interaction between the Cr magnetic moments. Therefore, modifications in the (Te,Se) sub-lattice, which are small at low Se content, can become important for further substitution of Te atoms by Se and can be responsible for the properties of the $Cr_{(1+x)}Q_2$ system discussed here. These modifications are related among others to the remarkable difference in the size of Te and Se atoms that is reflected by the different lattice parameters of the ordered CrTe and TeSe compounds. A random distribution of Te and Se atoms and the decrease of the lattice parameter *a* (reflecting the average size of (Te, Se) atoms) upon substitution of Te atoms by Se, result in the creation of the local stresses and distortions in the lattice. Only the averaged positions of (Te, Se) atoms in a unit cell determined in the experiment enter our calculations. However, local distortions may be more pronounced than the average ones. Also the shifts of Te and Se atoms should be different because of their different size. These shifts should result in a modification of the exchange coupling because of dependence of the hybridization of Te and Se *p*-states and Cr *d*-states on the relative positions of the atoms, which is not taken into account in present calculations.

Distortions within the (Te,Se) sub-lattice should influence also the distribution and ordering of Cr atoms and can result in their redistribution between the fully occupied and partially occupied sub-lattices. To investigate the influence of such redistribution on the exchange coupling constants, these were recalculated assuming a transfer of 10% of Cr atoms from the fully occupied sub-lattice to the partially occupied one. Their values as a function of the Fermi energy are plotted in Fig. 17 (dashed lines), which shows only minor modifications for the exchange interaction. The energy of a distorted lattice can also be decreased through relaxations caused by vacancies appearing in the (Te, Se) sub-lattice. In this case one can expect an increase for the number of vacancies together with the occupation of the incomplete Cr(2) sub-lattice, which restrict the possible relaxations related to the shifts of Te and Se atoms along the *c*-axis. Fig. 18 shows that the introduction of 5% of vacancies results in pronounced changes concerning the magnitude of the exchange coupling parameters that can result in appreciable changes of the critical temperature.

While our calculations of the exchange coupling parameters and the subsequent MC simulations give already a qualitative explanation for the variation of T_c with Cr content (see Fig. 16), our model considerations for the coupling parameters supply a possible explanation for the steep increase of T_c found in experiment. Further MC simulations, that however have to use larger repeat units, should allow confirming the expectations.

4. Conclusions

The results of the present study support the tendency of the changes of the magnetic properties experimentally determined in our previous study. For very similar Cr contents the Weiss constant θ becomes more negative, i.e., a higher Se concentration induces stronger antiferromagnetic exchange interactions and weakens the ferromagnetic exchange. The same trend is observed for the Curie temperature T_c [17,18]. With increasing Se content the value for T_c decreases for compounds with a similar Cr concentration. The substitution of Te by Se shortens the distances

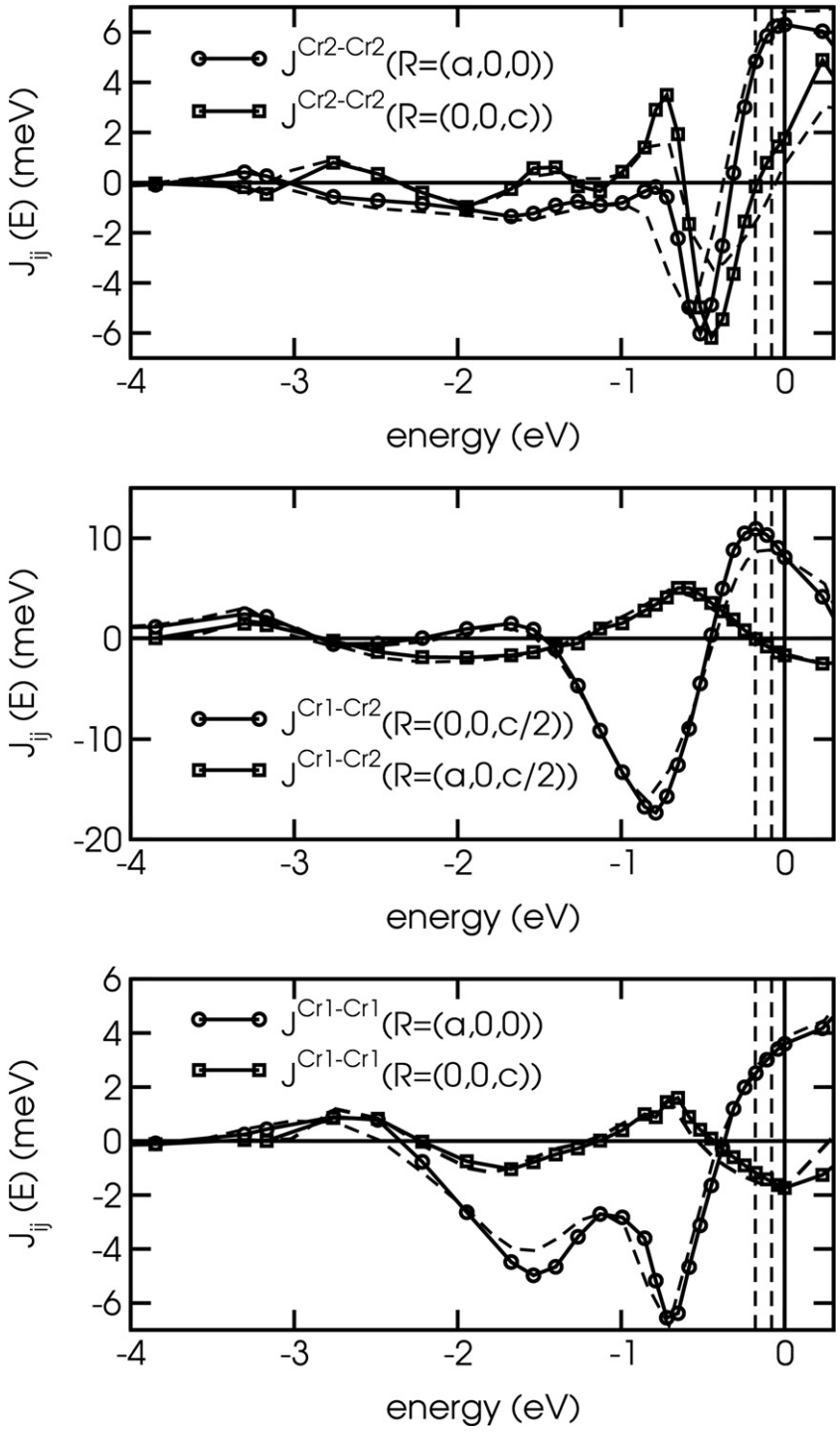

Fig. 17. The $J^{Cr1-Cr1}$, $J^{Cr1-Cr2}$ and $J^{Cr2-Cr2}$ exchange coupling parameters between the first and second neighbors as a function of the Fermi energy.

between neighbored Cr atoms thus strengthening the direct antiferromagnetic exchange interactions. Independent from the Te:Se ratio the compounds with the lower Cr content exhibit a SG or SG-like behavior whereas the Cr richer samples behave like CGs or ferromagnetic materials. Furthermore, as for the other two investigated Te:Se ratios (7:1 and 6:2), the HT modification exhibit stronger magnetizations than the LT compounds. This finding can be rationalized on the basis of the more regular angles Cr–*Q*–Cr and shorter Cr–Cr separations. According to the experimental results the homogeneity range of the phases seem to extend to higher Cr concentrations with increasing Se content. SPR-KKR-CPA band-structure calculations yield a more qualitative and detailed description of the experimentally observed magnetic data. The MC simulations revealed in particular that the critical temperature T_c increases with increasing Cr contents even though both experimental and theoretical values do not match perfectly. Further investigations with samples having larger unit cells are in progress to confirm this observation. The above results enable us to confirm the effects of Se concentration and Cr content onto the magnetic properties of the $Cr_{(5+x)}Te_{8-y}Se_y$ series. Further

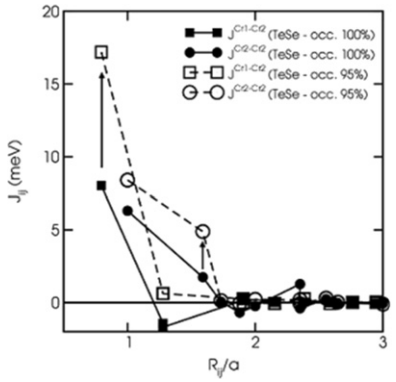

Fig. 18. Comparison of the exchange coupling parameters for $Cr_{1.41}Q_2$ with fully occupied (Te, Se) sub-lattice (solid lines) and with 5% vacancies in (Te, Se) sub-lattice (dashed lines). The inter-atomic distances are represented in units of lattice parameters *a*.

studies in the system with a very low Te content (e.g. Te:Se = 1:7) are under way because this will assist to understand the behavior of the (Te,Se) sub-lattice onto the final magnetic properties.

Acknowledgments

The authors thank Ms. Rasmussen (Institute of Inorganic Chemistry, University of Kiel) for the magnetic measurements, Dr. Dieter Garbe-Schönberg (Institute of Geochemistry, University of Kiel) for the ICP analysis. The DFG is acknowledged for the financial support by the SPP 1136 project (BE 1653/12-2).

References

[1] V.A. Gordienko, V.V. Zubenko, V.I. Nikolaev, Zh. Eksp. Teor. Fiz. 57 (1969) 1597–1600.
[2] M. Rosenberg, A. Knülle, H. Sabrowsky, C. Platte, J. Phys. Chem. Solids 43 (1982) 87–95.
[3] J.H. Zhang, T.L.T. Birdwhistell, C.J. O'Connor, Solid State Commun. 74 (1990) 443–446.
[4] K. Hatakeyama, T. Taneko, H. Yoshida, S. Ohta, S. Anzai, J. Magn. Magn. Mater. 90–91 (1990) 175–176.
[5] K. Yaji, A. Kimura, Ch. Hirai, M. Taniguchi, M. Koyoma, H. Sato, K. Shimada, A. Tanaka, T. Muro, Sh. Imada, Sh. Suga, Phys. Rev. B 70 (2004) 064402-1–064402-7.
[6] H. Haraldsen, A. Neuber, Z. Anorg. Allg. Chem. 234 (1937) 353–371;
K. Ozawa, T. Yoshimi, M. Irie, S. Yanagisawa, Phys. Stat. Sol. 11 (1972) 581–588;
T. Kanomata, Y. Sugawara, K. Kamishima, H. Mitamura, T. Goto, S. Ohta, T. Kaneko, J. Magn. Magn. Mater. 177–181 (1998) 589–590.
[7] A.W. Sleight, T.A. Bither, Inorg. Chem. 8 (1969) 566–569.
[8] M. Yuzuri, N. Nakamura, J. Phys. Soc. Jpn. 19 (1964) 1350–1354.
[9] T.J.A. Popma, C. Haas, B. van Laar, J. Phys. Chem. Solids 32 (1971) 581–590;
D. Babot, M. Chevreton, J. Solid State Chem. 8 (1973) 166–174.
[10] M. Yuzuri, T. Kaneko, T. Tsushima, S. Miura, S. Abe, G. Kido, N. Nakagawa, J. Phys. C 8 (1988) 231–232;
P. Vaqueiro, A.V. Powell, A.I. Coldea, C.A. Steer, M.I. Marshall, S.J. Blundell, I. Singleton, T. Ohtani, Phys. Rev. B 64 (2001) 132402-1–132402-4.
[11] M. Chevreton, M. Murat, C. Eyraud, E.F. Bertaut, J. Phys. 24 (1963) 443–446.
[12] M. Yuzuri, J. Phys. Soc. Jpn. 35 (1973) 1252.
[13] T. Kaneko, J. Sugawara, K. Kamigaki, S. Abe, H. Yoshida, J. Appl. Phys. 53 (1982) 2223–2225.
[14] Y. Adachi, M. Yuzuri, T. Kaneko, S. Abe, H. Yoshida, J. Phys. Soc. Jpn. 63 (1994) 369–370.
[15] Y. Adachi, M. Ohashi, T. Kaneko, M. Yuzuri, Y. Yamaguchi, S. Funahashi, Y. Morii, J. Phys. Soc. Jpn. 63 (1994) 1548–1559.
[16] K. Lukoshus, S. Kraschinski, C. Näther, W. Bensch, R.K. Kremer, J. Solid State Chem. 177 (2004) 951–959.
[17] Zh.-Le Huang, W. Bensch, D. Benea, H. Ebert, J. Solid State Chem. 177 (2004) 3245–3253.
[18] Zh.-Le Huang, W. Bensch, S. Mankovsky, S. Polesya, H. Ebert, R.K. Kremer, J. Solid State Chem. 179 (2006) 2067–2078.
[19] J. Rigoullt, C.-G. Morosini, A. Tomas, P. Molinie, Acta Crystallogr. B38 (1982) 1557–1559.
[20] H.M. Rietveld, J. Appl. Crystallogr. 22 (1967) 151–152.
[21] H.M. Rietveld, J. Appl. Crystallogr. 2 (1969) 65–71.
[22] D.B. Wiles, R.A. Young, J. Appl. Crystallogr. 14 (1981) 149–151.
[23] R.J. Hill, C.J. Howard, J. Appl. Crystallogr. 20 (1987) 467–474.
[24] J. Rodriguez-Carvajal, Fullprof. 2k, Version 2.0c—July 2002/Lab. Leon Brillouin, 2002.
[25] W. Bensch, O. Helmer, C. Näther, Mater. Res. Bull. 32 (1997) 305–318.
[26] J.-F. Bérar, P. Lelann, J. Appl. Crystallogr. 24 (1991) 1–5.
[27] J. Korringa, Physica 13 (1947) 392–400.
[28] W. Kohn, N. Rostoker, Phys. Rev. 94 (1954) 1111–1120.
[29] H. Ebert, et al., The Munich SPR-KKR package, version 2.1.1, 〈http://olymp.cup.uni-meunchen.de/ak/ebert/SPRKKR〉.
[30] H. Ebert, in: H. Dreyssé (Ed.), Electronic Structure and Physical Properties of Solids, Springer, Berlin, 2000, p. 191.
[31] S.H. Vosco, L. Wilk, M. Nusair, Can. J. Phys. 58 (1980) 1200–1211.
[32] P. Soven, Phys. Rev. 156 (1987) 809–813.
[33] G.M. Stocks, W. Temmerman, B.L. Gyorffy, Phys. Rev. Lett. 41 (1978) 339–343.
[34] A.I. Lichtenstein, M.I. Katsnelson, V.P. Antropov, V.A. Gubanov, J. Magn. Magn. Mater. 67 (1987) 65–74.
[35] A. Hayashi, Y. Ueda, K.A. Kosuge, H. Murata, H. Asano, N. Watanabe, F. Izumi, J. Solid State Chem. 67 (1987) 346–353.
[36] K.O. Klepp, H. Boller, J. Solid State Chem. 48 (1983) 388–395;
W. Bensch, C. Näther, O. Helmer, C. Ritter, J. Alloys Compd. 2990 (1999) 41–51.
[37] W. Bensch, E. Wörner, M. Muhler, U. Ruschewitz, J. Solid State Chem. 110 (1994) 234–242;
R. Quint, H. Boller, Mater. Res. Bull. 22 (1987) 1499–1504.
[38] W. Bensch, B. Sander, C. Näther, R.K. Kremer, C. Ritter, Solid State Sci. 3 (2001) 559–568.
[39] R.D. Shannon, Acta Crystallogr. A32 (1976) 751–767.
[40] W. Bensch, B. Sander, R.K. Kremer, W. Kockelmann, J. Solid State Chem. 158 (2001) 198–207 (and references therein).
[41] K. Shimada, T. Saitoh, H. Namatame, A. Fujimori, S. Ishida, S. Asano, S. Anzai, Phys. Rev. 53 (1996) 7673–7683.
[42] J.B. Goodenough, J. Phys. Rev 100 (1955) 564–573.
[43] J.B. Goodenough, J. Phys. Chem. Solids 6 (1958) 287–297.
[44] J. Kanamori, J. Phys. Chem. Solids 10 (1959) 87–98.
[45] S. Nagata, P.H. Keesom, H.R. Harrison, Phys. Rev. B 19 (1979) 1633–1638;
J.A. Mydosh, Spin Glasses: An Experimental Introduction, Taylor & Francis, London, 1993.
[46] A. Ito, H. Aruga, E. Torikai, M. Kikuchi, Y. Syono, H. Takei, Phys. Rev. Lett. 57 (1986) 483–486.